Korean J. Chem. Eng., 36(6), 860-868 (2019)
DOI: 10.1007/s11814-019-0265-3

pISSN: 0256-1115
eISSN: 1975-7220

Trimellitic acid functionalized magnetite nanoparticles for the efficient removal of Pb(II) and Cr(VI) from wastewater streams

Tehreema Nawaz*, Mudassir Iqbal*, Sonia Zulfiqar, and Muhammad Ilyas Sarwar***,†**

*Department of Chemistry, School of Natural Sciences, National University of Sciences and Technology, H-12, Islamabad 44000, Pakistan
**Department of Chemistry, School of Sciences & Engineering, The American University in Cairo, New Cairo 11835, Egypt
***Department of Chemistry, Quaid-i-Azam University, Islamabad 45320, Pakistan
(*Received 23 August 2018 • accepted 8 April 2019*)

Abstract−Silica-coated Fe_3O_4 nanoparticles were prepared and functionalized with trimellitic anhydride generating novel amide and two acid moieties on the surface of the nanoparticles. These nanoparticles were found to be ferrimagnetic with average particle size 50-60 nm as characterized by XRD, SEM, EDS, VSM and FTIR analyses. The functionalized nanoparticles were exploited as adsorbent for the removal of Pb(II) cations and Cr(VI) anions from their aqueous solutions and uptake of metal ions was monitored by atomic absorption spectroscopy (AAS). These nanoparticles were found to be more effective for the removal of Pb(II) cations due to the negatively charged surface groups relative to Cr(VI) anions. The adsorption data fitted well with Langmuir as well as Freundlich adsorption isotherms, showing a complex nature of adsorption phenomena, comprising electrostatic as well as chemical attraction between surface groups and metal ions. The metal bearing nanoparticles were easily separated from the solution by simply applying external magnetic field.

Keywords: Fe_3O_4 Nanoparticles, Functionalization of Fe_3O_4, Ferrimagnetic Nano-sorbents, Adsorption of Pb(II) & Cr(IV), Easy Isolation by EMF

INTRODUCTION

Global industrial growth is primarily responsible for most of the natural and biological toxicity issues, originating from the discharge of pollutants, including dangerous heavy metal ions (chromium, cadmium, nickel, lead, zinc, arsenic, mercury etc.). These metal ions are thought to be very toxic for all living organisms. Their existence in the wastewater is mainly due to various ongoing chemical processes such as electroplating, metallurgical work, tanning, mining, batteries processing and metal plating. Some metals are highly toxic if present even at very minute levels [1]. Several techniques have been employed for the removal of hazardous metal ions like precipitation, filtration, osmosis, coagulation, flotation, flocculation and electrochemical treatment, etc. However, these methods have limitations as well due to low efficiency, secondary sludge generation, less selectivity, complex operating mechanisms and higher cost issues [2,3].

To overcome the above-mentioned constraints, recently, adsorption is preferred due to its selectivity, ease of handling and less secondary waste generation [4]. Moreover, availability of different adsorbents has made this method exceptionally reasonable for wastewater treatment. Further, surface area can be extensively increased by fabrication of these sorbents at nanoscale and their sizes can be tuned easily. Magnetic adsorbents are unique in this category to treat wastewater where a base adsorbent is implanted with oxides of metals like iron, nickel, copper and cobalt. After treatment, the magnetic nature of such adsorbents helps for easy isolation through an external magnetic field [5]. In this regard, iron oxide nanomaterials have been investigated; where large surface area and magnetic properties are simultaneously achieved [6-9]. Moreover, they are biocompatible, inert, less toxic and can be easily synthesized and modified for further applications. Usually, for better activity and mobility of these nanomaterials, various stabilizers have been used. But, due to biocompatibility and cost effectiveness, mesoporous silica coating is the most widely used method [10].

Moreover, the adsorption ability of coated nanoparticles can be improved by inducing target specific functionalities on its surface. For this propose, hydroxyl group of silica shell undergoes coupling reaction for surface modification with reactive amine groups that further facilitate the introduction of different functional groups on the surface of magnetic nanoparticles. Iron-based nanoparticles are prone to acid attack and damaged under acidic environment. Therefore, silica coating helps to protect the magnetic core as it is stable under various reaction media [11-13].

This article presents a synthesis of amino terminated silica coated magnetic nanoparticles, which were further modified to trimellitic acid functionalised magnetite nanoparticles by reacting them with trimellitic anhydride. Trimellitic acid functionalised magnetite nanoparticles (FTA-1) were synthesized for the first time and used as nano-adsorbents for the removal of Pb(II) and Cr(VI) from the aqueous solutions under optimized parameters. This work is useful for understanding the detailed adsorption behavior and

†To whom correspondence should be addressed.
E-mail: ilyassarwar@hotmail.com, ilyas@qau.edu.pk

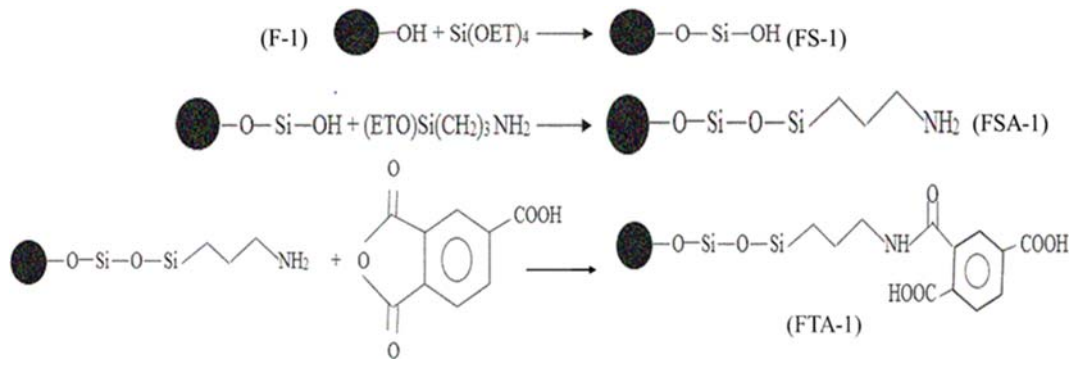

Fig. 1. Reaction scheme for the synthesis of functionalized nanoparticles.

mechanism of magnetic nano-sorbents.

EXPERIMENTAL SECTION

1. Materials

All the chemicals, including ferrous sulfate hepta hydrate ($FeSO_4 \cdot 7H_2O$), tetraethylorthosilicate (TEOS), aminopropyltriethoxysilane (APTES), ethanol, toluene, potassium hydroxide, potassium nitrate, tetrahydrofuran (THF), trimellitic anhydride, phosphoric acid, boric acid, acetic acid, sodium hydroxide, lead nitrate and potassium dichromate were purchased from commercial sources. All the chemicals and solvents were of reagent grade and were used without further purification. Solvents were dried according to standard procedures and stored over molecular sieves.

2. Synthesis of Trimellitic Acid Functionalized Fe_3O_4 (FTA-1)

2-1. Synthesis of Magnetite Nanoparticles (F-1)

Oxidative hydrolysis route was used for the synthesis of Fe_3O_4 nanoparticles, where hydrolysis of Fe(II) salt was carried out in the presence of a strong oxidizing agent (KNO_3) as previously reported [14]. Synthesis involved the dissolution of $FeSO_4 \cdot 7H_2O$ (4 g) in deionized water (24 mL) into a three-neck round bottom flask, followed by slow addition of KOH (2.246 g per 12 mL of deionized water) and KNO_3 (0.324 g per 12 mL of deionized water) solutions under N_2 bubbling at 80 °C for 2 hrs. Then the reaction mixture was kept for 24 hrs at room temperature and nanoparticles (named as F-1) were washed several times with deionized water and dried at 60 °C [14].

2-2. Coating of Magnetite Nanoparticles (FS-1)

Fe_3O_4 nanoparticles were coated with silica using sol-gel technique. In this process, first Fe_3O_4 nanoparticles (125 mg) were dispersed in ethanol (94 mL) in an ultrasonic bath for 30 min, followed by the addition of ammonium solution (7.5 mL) as catalyst and tetraethylorthosilicate (0.25 mL). This solution was further sonicated in ice bath for 2 hrs. Finally, silica coated nanoparticles were separated, washed, dried in vacuum oven at 60 °C and designated as FS-1 [15].

2-3. Amino-modification of Silica Coated Magnetite Nanoparticles (FSA-1)

For amino modification, FS-1 nanoparticles (100 mg) were agitated for 1 h in toluene (100 mL), followed by the addition of 3-aminopropyl triethoxysilane (3 mL). Then the reaction mixture was refluxed under nitrogen for 24 hrs. These amino-modified nanoparticles were washed and dried under vacuum at 60 °C, abbreviated as FSA-1 [16].

2-4. Trimellitic Acid Functionalized Amino-modified Magnetite Nanoparticles (FTA-1)

FSA-1 nanoparticles (100 mg) were dispersed in THF (50 mL) and stirred for 15 min. To this mixture, trimellitic anhydride (200 mg) was added and reaction was agitated for 1 h followed by addition of trimethylamine (1 mL). This reaction mixture was refluxed for 10 hrs at 60 °C and functionalized nanoparticles were washed and dried at 60 °C under vacuum, labelled as FTA-1. The reaction scheme for the formation of functionalized nanoparticles is given in Fig. 1.

3. Characterization of Nanoparticles

Phase identification and crystallinity of all the samples (F-1, FS-1 and FTA-1) was monitored using an X-ray Diffractometer D8 Advanced Davinci by Bruker having Cu kα radiation (1.54 Å) and operated at 40 KV voltage and 30 mA currents. For morphological studies, scanning electron microscope MIRA3 TESCAN operated at 10 kV voltages was used. Energy dispersive X-ray spectroscopy (EDS), a technique coupled with SEM, was used for elemental analysis of the samples. PLATINUM-ATR ALPHA (BRUKER) was used for functional group determination of the powder samples in the range of 4,000-500 cm^{-1}. Zeta potential of the sample was measured using Malvern Panalytical zeta potential analyzer. To determine the Brunauer-Emmett-Teller (BET) surface area of FTA-1, N_2 adsorption isotherms at 77 K were obtained using a Micromeritics Gemini VII 2390 surface area analyzer. Magnetic measurements were performed on vibrating sample magnetometer The Lake Shore VSM 7407, using a saturation magnetization value between −10 kOe to 10 kOe at room temperature. Finally, for adsorption studies, uptake of metal ions was measured by flame atomic absorption spectrometer (Shimadzu AA-670).

4. Adsorption Efficiency

Batch equilibrium technique was used in aqueous solutions for optimization of different adsorption parameters (time, pH, concentration of ions) and for the calculation of percentage adsorption efficiency and equilibrium adsorption capacity (q_e). Briefly, 10 mg of nanoparticles were added into 10 mL solution of known concentrations of metal ions (10 ppm, 20 ppm, 30 ppm, 40 ppm and 50 ppm) and agitated in a shaker at 125 rpm until equilibrium was reached. Then sorbent was magnetically removed from aqueous solutions, and the remaining metal ions concentration was investi-

gated in elute by AAS. Percent adsorption and equilibrium adsorption limit were calculated using formulae as given below.

$$\% \text{ Removal} = \frac{C_i - C_e}{C_i} * 100 \quad (1)$$

$$q_e = \frac{(C_i - C_e)V}{M} \quad (2)$$

where C_i is the initial metal ions concentration in gL^{-1}, C_e is equilibrium concentration of metal ions in gL^{-1}, V is volume of solution in litre and M represents the mass of adsorbent FTA-1 in grams.

RESULTS AND DISCUSSION

1. Phase Determination and Morphology of Nanoparticles

Phase and crystallographic structure of prepared nanoparticles were analyzed using X-ray diffraction technique, and measurements were performed for 2θ in the range of 25° to 70° on powered samples. Fig. 2 presents X-ray diffraction patterns of naked, coated and functionalized nanoparticles. Various peaks appeared at 30.1, 35.5, 37.1, 43.1, 53.5, 57.0 and at 52.6 (2θ) having (220), (311), (222), (400), (422), (511) and (440) hkl values. The representative XRD patterns demonstrate the single-phase materials and exhibit the typical diffraction pattern of magnetite crystal structure as given in the JCPDS 01-075-0033 powder diffraction, but still the possibility of the formation of maghemite cannot be excluded fully as it shows the almost same XRD pattern. Furthermore, diffractograms clearly indicate a well retained crystalline phase of naked magnetite nanoparticles, and no peak shift is observed subsequently upon coating and functionalization. Therefore, the crystalline phase and stability of Fe_3O_4 nanoparticles remain unaffected. Moreover, XRD data was used to calculate the crystallite size of Fe_3O_4 nanoparticles by using Scherer formula and the average particle size was 45.08 nm.

The surface morphology of prepared nanoparticles was investigated through scanning electron microscopy. A microscopic analysis was performed on the powered samples and micrographs are presented in Fig. 3. The morphology of naked magnetite nanoparticles was also compared with the coated and functionalized nanomaterials. SEM images clearly indicate a cubic morphology for naked magnetite nanoparticles with an average particle size 53.5± 5.5 nm which agrees with the crystallite size calculated by XRD as these particles are seemed to stack together in the agglomerated form. After silica coating, the morphology of magnetite nanoparticles slightly changes from cubical to spherical shape (see Fig. 3(c)-(d)). These observations are in accordance with the previous studies [17]. Fig. 3(c)-(f) shows the coated and functionalized materials due to the presence of amorphous functionalities on their surface forming a cloud-like shell around magnetite nanoparticles. The amorphous silica shell around magnetite (FS-1) gave a cloudy appearance (Fig. 3(c)-(d)); this cloudy appearance became thicker and thicker when silica coated particles were modified with NH_2 (Fig. 3(e)) and trimellitic acid (FTA-1) functionalities (Fig. 3(f)). In case of FTA-1, even more thickness of cloudy shell may be seen due to the presence of bulky groups on the particle's surface without affecting the crystalline phase and stability of Fe_3O_4 nanoparticles.

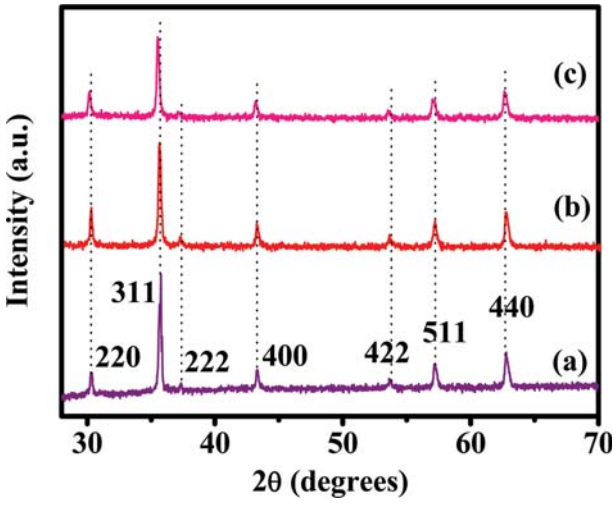

Fig. 2. XRD patterns of the naked (a) F-1, coated (b) FS-1 and functionalized (c) FTA-1 magnetite nanoparticles.

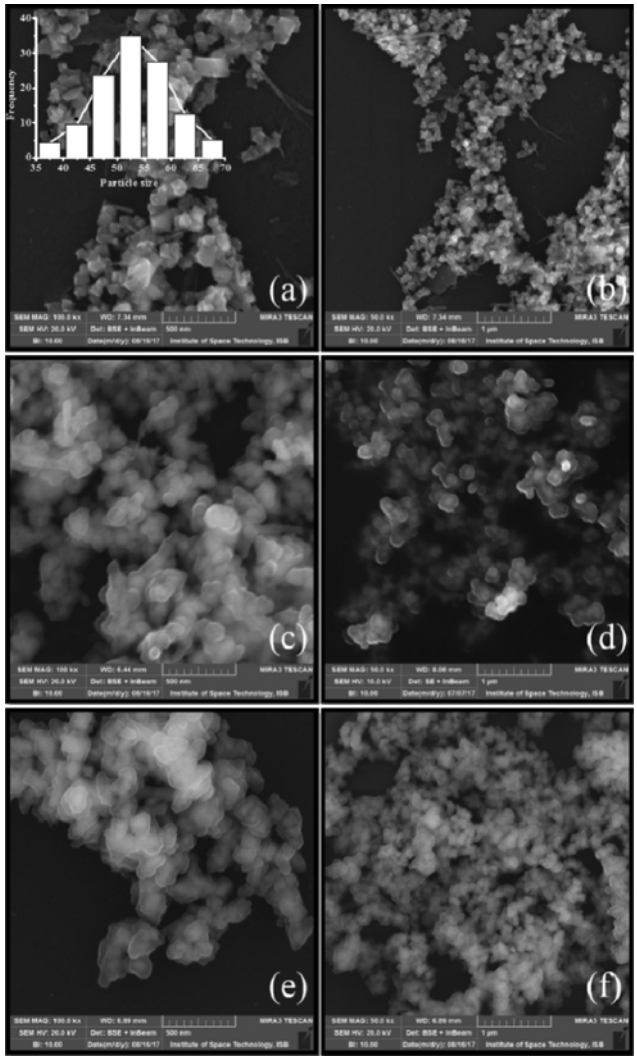

Fig. 3. SEM micrographs of naked (a)-(b) F-1, coated (c)-(d) FS-1 and functionalized (e)-(f) FTA-1magnetite nanoparticles.

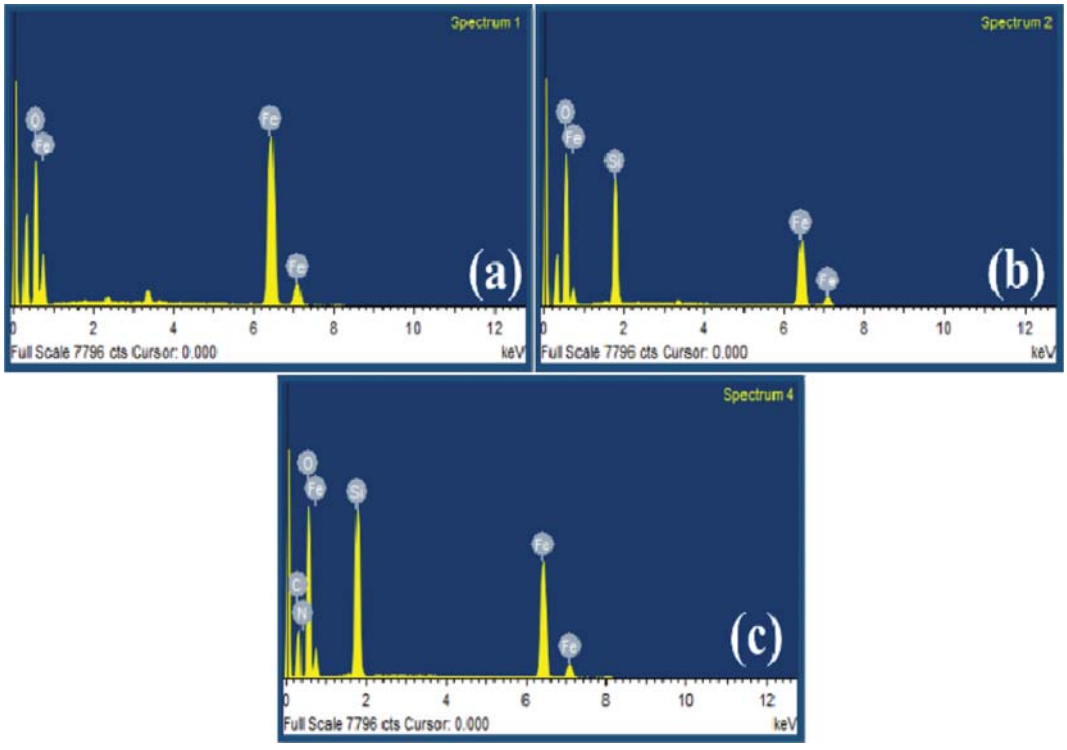

Fig. 4. EDS spectra of the naked (a) F-1, coated (b) FS-1 and functionalized (c) FTA-1 magnetite nanoparticles.

2. Chemical Composition and Surface Groups Determination

Energy-dispersive X-ray spectroscopy is useful for elemental analysis or chemical composition of a sample. The same technique was used to determine the elemental composition of the nanoparticles, and the EDS spectra recorded are given in Fig. 4. Two elements Fe and O are present in pure magnetite spectrum (Fig. 4(a)) and the elemental composition confirmed the purity of the sample with 27.07 and 72.93 weight percent of O and Fe, respectively. EDS spectrum (b) shows an additional Si peak confirming the surface coating of magnetite nanoparticles. Elemental composition of the same sample also gave 17.92 weight percent of silica but percentage of O was increased in comparison with Fe due to surface coating of pure magnetite with silica. Fig. 4(c) demonstrates two additional peaks for carbon and nitrogen, verifying the successful modification and functionalization of nanomaterials. Here again, percentage of O was found to be increased due to the presence of surface carboxylic groups in the functionalized nanoparticles.

The formation of magnetite nanoparticles and their subsequent coating, modification and functionalization was ascertained by recording their IR spectra (Fig. 5), and characteristic band at 550 cm^{-1} was assigned to Fe-O stretching vibration confirming the formation of Fe_3O_4 nanoparticles. Surface coating with TEOS gave two bands at 790 and 1,065 cm^{-1} due to Si-O and Si-O-Si stretching vibrations, respectively, in both coated (FS-1) and amine modified (FSA-1) nanomaterials. A new band appeared at 1,629 cm^{-1} in spectrum of amine modified nanoparticles due to N-H bending vibration. In functionalized sample (FTA-1), a band appeared between 1,702-1,722 cm^{-1} of C=O stretching due to the presence of acid moiety. Other bands emerged at (690, 800-944, 1,280, 1,400-1,620, 1,655, 1,687, 2,000-1,050, 2,950-3,100) cm^{-1} due to C=C (oop bend), C-H (oop bend), C=C (str), amide N-H (bend), amide C=O (str), ring overtones and C-H (str), respectively. The IR data confirms the successful coating, modification and functionalization of magnetite nanoparticles.

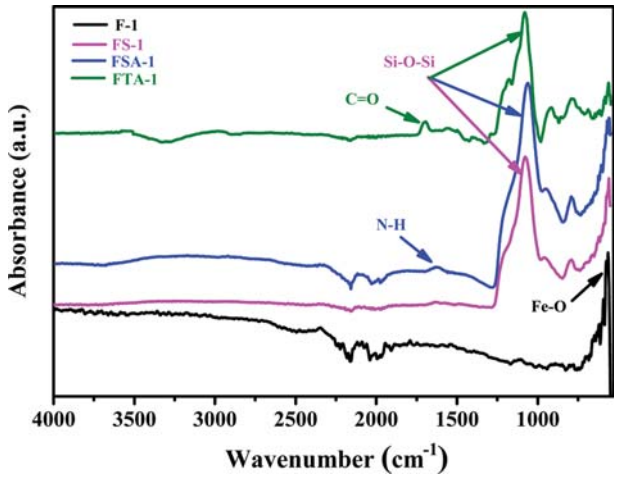

Fig. 5. FTIR spectra of naked, coated, modified and functionalized nanoparticles.

3. Zeta Potential and Surface Area Measurements

Zeta potential studies and N_2 adsorption-desorption isotherms were used to evaluate the surface charge, surface area and pore structure of FTA-1 adsorbent. The surface charge on FTA-1 at pH 7 is shown in Fig. 6. The zeta potential at pH 7 is negative (–8.01), which is expected due to presence of carboxylate anions on the surface. This also correlates with the adsorption studies performed on

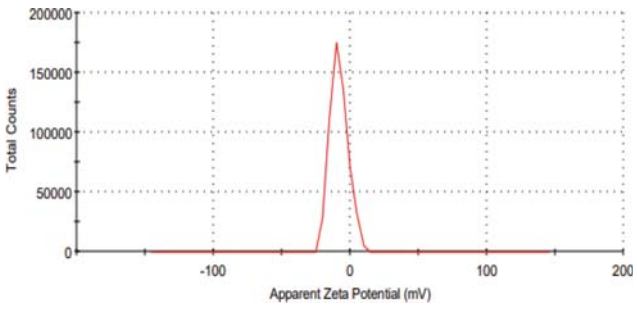

Fig. 6. Zeta potential of FTA-1.

metal ions at various pH values. As the surface is found to be negatively charged at neutral pH due to ionization of carboxylic acid, preferential adsorption of Pb(II) ions is expected compared to Cr(VI) anions. No considerable change for Pb(II) adsorption was observed at higher pH values; however, the adsorption of Cr(VI) was decreased further. At lower pH values, the surface is expected to be protonated, which will favor adsorption of Cr(VI) anions more as compared to Pb(II) cations. The same trend has been observed while moving from higher to lower pH values. Moreover, BET was used to determine the surface area. The surface area was found to be 3.66 m^2/g. This value is in favor of electrostatic adsorption phenomena, as surface area of nanoparticles is less due to more size and more functionality on the surface. However, physisorption cannot be neglected completely and seems more favorable in case of Cr(VI) anion [18-20].

4. Magnetic Measurements

VSM technique is basically employed to measure the magnetic properties of the materials. Fig. 7 describes the magnetic measurements and hysteresis loops of pure and functionalized magnetite nanoparticles. The mass saturation magnetization value (M_s) for pure magnetite was found to be 65.96 emu/g relative to the bulk value of Fe_3O_4 (90 emu/g) [21]. However, this value is higher than the values already reported in literature [22-26]. A decrease in M_s value from 65.96 to 48.50 emu/g for FTA-1 was observed and considered due to the contributions of non-magnetic silica/amino/

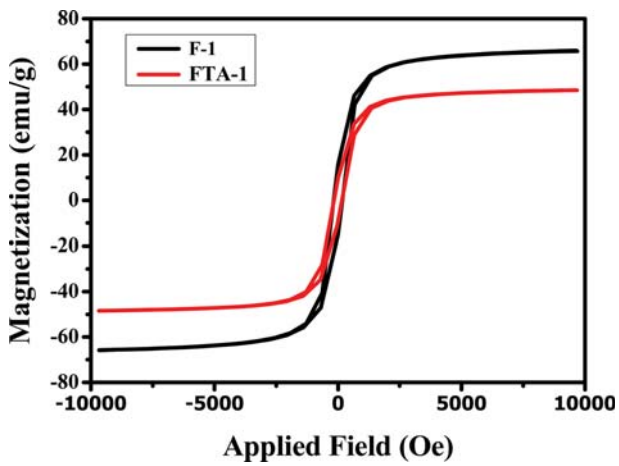

Fig. 7. VSM measurements of naked and functionalized magnetite nanoparticles.

Table 1. VSM parameters of naked and functionalized magnetite nanoparticles

Sample	F-1	FTA-1
M_s (emu/g)	65.96	48.50
M_r (emu/g)	15.764	9.59
SQD	0.238	0.197
H_c (O_e)	247.25	206.65

trimellitic acid shell to the total mass of the nanoparticles. These results are analogous to previously studied modified/functionalized systems [27]. The values of squareness ratios from Table 1 are 0.238, 0.197 for (F-1) and (FTA-1). Moreover, the size of these prepared nanoparticles was more than the threshold value (>25 nm) for superparamagnetic behavior and they showed high values of coercivity and remetization magnetization, that is favored for ferrimagnetic behavior [28-32].

5. Adsorption Studies

Novel adsorbent (FTA-1) containing amide and two acid moieties on the surface tend to be an efficient chelating site for divalent cations. These adsorbents can be exploited for the removal of heavy metal ions from wastewater and further cleaning of the water effluents from industries. Lead and chromium have been chosen in the present study, which have the strong tendency to be chelated by amide and acid moieties present on the surface of functionalized nanoparticles. For adsorption measurements, different parameters were optimized for the uptake of metal ions like contact time, concentration of metal ions and pH.

5-1. Contact Time

Adsorption of lead ions was measured as a function of contact time. Lead solution (10 mL) of 10 ppm concentration was shaken with 10 mg of adsorbent at neutral pH and ambient temperature for different time intervals (15, 30, 60, 90 and at 120 min). Fig. 8 shows percent adsorption of Pb(II) ions by functionalized materials with time. Metal ions uptake was optimized and equilibrium was reached after 1 h. The same procedure was repeated for chromium ions at room temperature for different time intervals (1, 2,

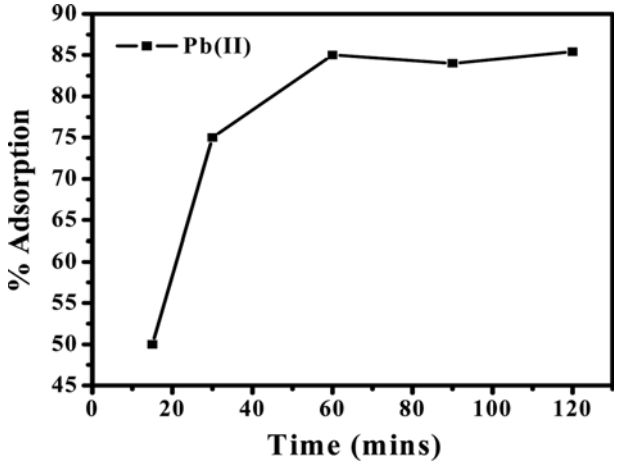

Fig. 8. Effect of contact time on adsorption capacity of Pb(II) ions (10 ppm solution of Pb(II) ions at room temperature and 7 pH).

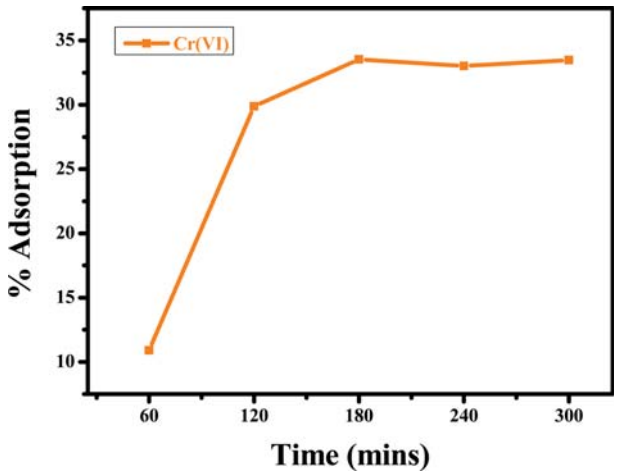

Fig. 9. Effect of contact time on adsorption capacity of Cr(VI) ions (10 ppm solution of Cr(VI) ions at room temperature and 7 pH).

3, 4 and 5 hrs); the adsorption trend is shown in Fig. 9. More adsorption capacity for Pb(II) cations with 90% removal after 1 h was observed relative to the Cr(VI) anions with maximum 35% removal after 3 hrs. This is because the surface of the adsorbent is more negatively charged due to the presence of one amide and two carboxylic groups attracting Pb(II) cations more than Cr(VI) anions. The repulsive forces between anions are more effective, reducing % adsorption of Cr(VI), and need more time for equilibrium to be reached.

5-2. pH

Metal complexation with functionalized nanoparticles is pH sensitive and metal ion uptake is improved with increasing pH of the system at room temperature and optimized values of time: 1 hour for Pb(II) ions and 3 hours for Cr(VI) ions. At lower pH, H^+ ions competed with Pb^{2+} cations for interaction on the adsorbents surface and adsorption was nearly negligible at lower pH values because at pH 2-3, the adsorbent surface remained protonated. When pH started increasing from 4-6, a drastic change was observed in the adsorption rate because the influence of H^+ ions became less significant and the interaction of Pb(II) with the adsorbent increased and optimum adsorption was found at pH 6 (Fig. 10). Moreover, net negative charge of two carboxyl groups and amide group also causes chelation with the Pb^{2+} and more than 85% removal of Pb(II) was observed at this particular pH value. At higher pH, OH^- ions started interfering with the Pb^{2+} cations and precipitated out as $Pb(OH)_2$. Different species of lead were supposed to be present in the aqueous solution, such as Pb^{2+} ions, $Pb(OH)^+$, $Pb(OH)_2^0$, $Pb(OH)_3^-$, $Pb(OH)_4^{-2}$ at higher pH, decreasing the adsorption capacity. Cr(VI) anions showed optimum adsorption at pH 3 and more than 60% Cr(VI) anions attracted by functionalized nanoparticles as given in Fig. 10. At lower pH, Cr(VI) ions exist in form of $HCrO_4^-/Cr_2O_7^{2-}$ and the surface of adsorbent is assumed slightly protonated due to the presence of high concentration of H^+ ions. It causes adsorption of $HCrO_4^-$ and $Cr_2O_7^{2-}$ at lower pH values, and the adsorption rate was negligible at higher pH values. Hydrogen bonding is another factor for the attraction of adsorbent to the adsorbate more towards itself. At lower pH, protonation of adsorbents allows them to make H-bonds with the adsorbate terminal charge. However, functionalized nanoparticles showed less adsorption of Cr(VI) anions even at lower pH values, because it is more negatively charged and more strongly acidic. It remains ionized even at pH 3 and less prone to protonation due to the presence of benzene ring.

5-3. Metal Ions Concentration

Concentration dependence of lead and chromium ions in terms of % adsorption was studied for various concentrations of these metal ions; 10, 20, 30, 40 and 50 ppm at optimised values of time: 1 h for Pb(II) and 3 h for Cr(VI) and pH i.e., 6 pH for Pb(II) and 3 pH for Cr(VI) ions. Optimum adsorption was recorded at 10 ppm, after that a decrease in uptake was observed (Fig. 11). This is due to the complexation of metal ions, which is completed at this concentration level; beyond that it showed a decreasing trend due

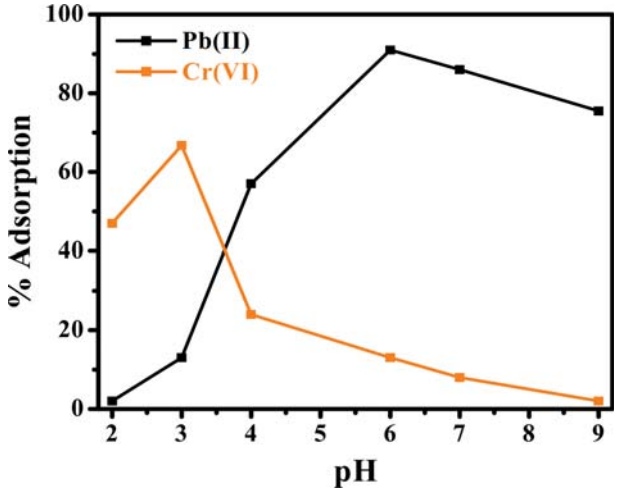

Fig. 10. Effect of pH on adsorption capacity of Pb(II) and Cr(VI) ions at room temperature and optimum values of time i.e. 1 hour for Pb(II) ions and 3 hours for Cr(VI) ions.

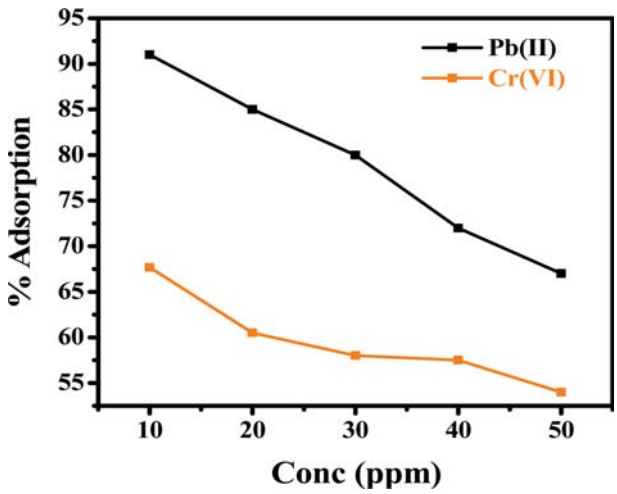

Fig. 11. Effect of metal ions concentration on adsorption capacity at optimum pH (6 pH for Pb(II) and 3 pH for Cr(VI) ions) and time (1 h for Pb(II) and 3 h for Cr(VI) ions).

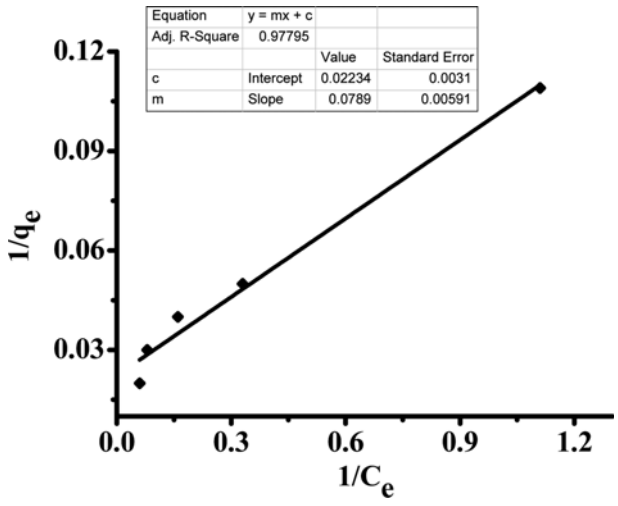

Fig. 12. Langmuir isotherm for the adsorption of Pb(II) on FTA-1.

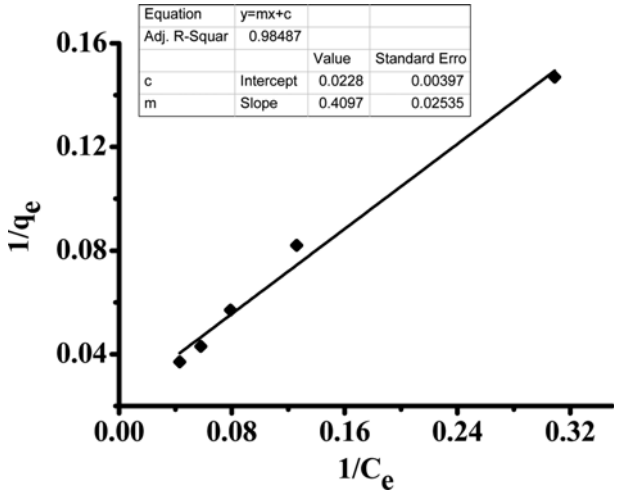

Fig. 13. Langmuir isotherm for the adsorption of Cr(VI) on FTA-1.

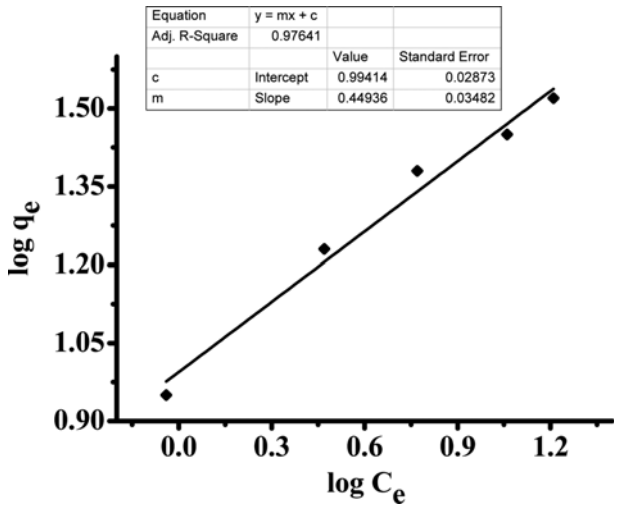

Fig. 14. Freundlich isotherm for adsorption of Pb(II) by FTA-1.

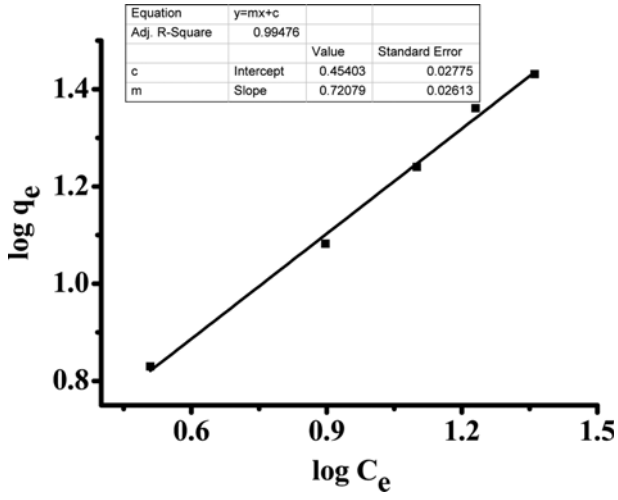

Fig. 15. Freundlich isotherm for adsorption of Cr(VI) by FTA-1.

Table 2. Langmuir isotherm parameters

FTA-1	Q_o (ml/g)	b or K_L (L/mg)	R^2	R_L
Pb(II)	62.76	0.28316	0.97795	0.07
Cr(VI)	43.85	0.055	0.98487	0.02

Table 3. Freundlich Isotherm parameters

FTA-1	K_f	1/n	R^2
Pb(II)	0.99414	0.44938	0.978
Cr(VI)	0.45403	0.72079	0.99476

to consumption of all the available sites or active sites became saturated with the metal ions. As there was no further vacant group which could be used for chelation of ions, adsorption efficiency decreased.

5-4. Isotherm Studies

Adsorption isotherms describe the adsorption behavior as well as the maximum adsorption capacity of adsorbent per metal ions concentration. Two adsorption models were applied, and the first model was the Langmuir adsorption isotherm. It is considered as an ideal adsorption model describing that adsorption on active sites is mono-layered, irreversible and homogeneous, and its parameters were studied using straight line equations (Figs. 12 & 13) for both ions and the values are shown in Table 2.

Another adsorption isotherm is the Freundlich adsorption model, which states that adsorption is reversible, multi-layered and heterogeneous. It is said to be non-ideal model for adsorption and its parameters are studied by straight line equation (Figs. 14 & 15) for both ions and their values are shown in Table 3. By comparing R^2 values, both isotherm models are in favor of adsorption, but the Freundlich adsorption isotherm is slightly preferable for these two adsorbents, as heterogeneous active sites are present on the adsorbent's surface and metals can be adsorbed by forming multi-layered surfaces on the adsorbent. The adsorption data fitted well with Langmuir as well as Freundlich adsorption isotherms, showing a complex nature of adsorption phenomena comprising chemical interactions. These results are completely in line with those

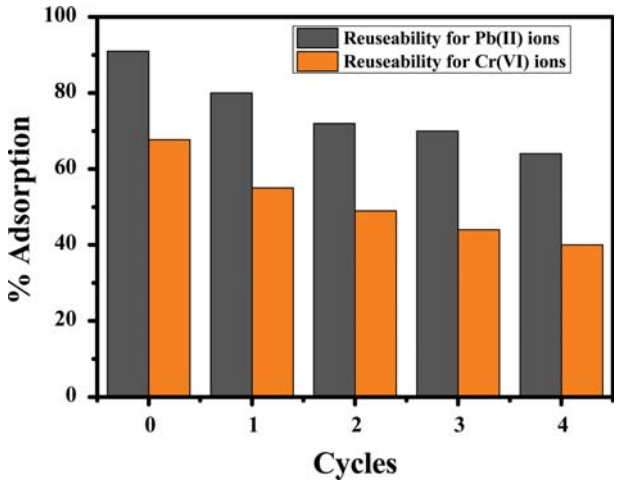

Fig. 16. Removal efficiency for Pb(II) and Cr(VI) ions on regenerated FTA-1 with evolution of adsorption-regeneration cycles.

described earlier in literature for magnetite materials [33].

5-5. Reusability of FTA-1

The recovery of adsorbent is a significant factor in practical use of the adsorbent. In this present study, suppressed adsorption of Pb(II) ions at lower pH values suggests that acid approach is feasible for the desorption and regeneration of FTA-1 sorbent. However, stability of nanosorbent under acidic conditions was determined by suspending FTA-1 in 0.5M HCl, and it was seen that less than 1% Fe content leached out from that medium. Since FTA-1 was stable under acidic environment, Pb(II) loaded adsorbent was regenerated by washing it with 0.5 M HCl and used for consecutive four cycles against Pb(II). The adsorption efficiency decreases in each cycle shown in (Fig. 16) due to protonation of adsorbent surfaces with H^+ ions in each cycle that decreases the Pb(II) ions adsorption on FTA-1. For Cr(VI) loaded adsorbent regeneration, 0.5 M NaOH was used and the adsorption efficiency followed the same trend in the four consecutive cycles (Fig. 14) showing the less availability of active sites and decrease in adsorption behaviour.

CONCLUSION

Novel trimellitic acid functionalized magnetite (FTA-1) nanoparticles were successfully synthesized and exploited for the removal of heavy metal ions from wastewater. Adsorption capacity of lead and chromium towards nanoparticles was studied through batch technique. The synthesized nanomaterials gave high adsorption capacity for Pb(II) cations and comparatively lower adsorption capacity for Cr(VI) anions from their aqueous solutions at optimised parameters. The interaction between the metal ions and adsorbent is both pH and time dependent. The results further show that the adsorbent is suitable practically at neutral as well as at acidic conditions. Moreover, experimental data well fitted with both Langmuir and Freundlich adsorption isotherms but more preferably with Freundlich adsorption isotherm, showing that removal of metal ions depends upon the physico-chemical interactions with the surface. The synthesized nano-adsorbent showed ferrimagnetic behavior and was easily separated by applying external magnetic field showing their great potential in wastewater treatment.

REFERENCES

1. S. O. Lesmana, N. Febriana, F. E. Soetaredjo, J. Sunarso and S. Ismadji, *Biochem. Eng. J.*, **44**, 19 (2009).
2. T. A. Kurniawan, G. Y. S. Chan, W. H. Lo and S. Babel, *Chem. Eng. J.*, **118**, 83 (2006).
3. F. Fu and Q. Wang, *J. Environ. Manage.*, **92**, 407 (2011).
4. E. Worch, *Walter de Gruyter.*, **344**, 321 (2012).
5. D. Mehta, S. Mazumdar and S. K. Singh, *J. Water Process Eng.*, **7**, 244 (2015).
6. B. M. Borah, B. Saha, S. K. Dey and G. Das, *J. Colloid Interface Sci.*, **349**, 114 (2010).
7. A. Durdureanu-Angheluta, A. Dascalu, A. Fifere, A. Coroaba, L. Pricop, H. Chiriac, V. Tura, M. Pinteala and B. C. Simionescu, *J. Magn. Magn. Mater.*, **324**, 1679 (2012).
8. E. Cheraghipour, A. M. Tamaddon, S. Javadpour and I. J. Bruce, *J. Magn. Magn. Mater.*, **328**, 91 (2013).
9. F. Keyhanian, S. Shariati, M. Faraji and M. Hesabi, *Arab. J. Chem.*, **9**, S348 (2016).
10. P. Xu, G. M. Zeng, D. L. Huang, C. L. Feng, S. Hu, M. H. Zhao, C. Lai, Z. Wei, C. Huang, G. X. Xie and Z. F. Liu, *Sci. Total Environ.*, **424**, 1 (2012).
11. C. Hui, C. Shen, J. Tian, L. Bao, H. Ding, C. Li, Y. Tian, X. Shi and H. J. Gao, *Nanoscale*, **3**, 701 (2011).
12. J. S. Lee, E. J. Lee and H. J. Hwang, *Trans. Nonferrous Met. Soc. China (English Ed.)*, **22**, s702 (2012).
13. M. Abbas, B. Parvatheeswara Rao, M. Nazrul Islam, S. M. Naga, M. Takahashi and C. Kim, *Ceram. Int.*, **40**, 1379 (2014).
14. A. Farrukh, A. Akram, A. Ghaffar, S. Hanif, A. Hamid, H. Duran and B. Yameen, *ACS Appl. Mater. Interfaces*, **5**, 3784 (2013).
15. F. Pena-Pereira, R. M. B. O. Duarte, T. Trindade and A. C. Duarte, *J. Chromatogr. A.*, **1299**, 25 (2013).
16. Y. Lin, H. Chen, K. Lin, B. Chen and C. Chiou, *J. Environ. Sci.*, **23**, 44 (2011).
17. C. Meng, W. Zhikun, L. Qiang, L. Chunling, S. Shuangqing and H. Songqing, *J. Hazard. Mater.*, **341**, 198 (2018).
18. M. E. Mahmoud, M. F. Amira, A. A. Zaghloul and G. A. A. Ibrahim, *Chem. Eng. J.*, **200-206**, 293 (2016).
19. K. Chen, J. He, Y. Li, X. Cai, K. Zhang, T. Liu, Y. Hu, D. Lin, L. Kong and J. Liu, *J. Colloid Interface Sci.*, **307-316**, 494 (2017).
20. Y. Liu, R. Fu, Y. Sun, X. Zhou, S. A. Baig and X. Xu, *Appl. Surface Sci.*, **267-276**, 369 (2016).
21. X. Batlle, N. Pérez, P. Guardia, O. Iglesias, A. Labarta, F. Bartolomé, L. M. Garca, J. Bartolomé, A. G. Roca, M. P. Morales and C. J. Serna, *J. Appl. Phys.*, **109**, 07B524 (2011).
22. L. Feng, M. Cao, X. Ma, Y. Zhu and C. Hu, *J. Hazard. Mater.*, **217-218**, 439 (2012).
23. S. Nigam, K. C. Barick and D. Bahadur, *J. Magn. Magn. Mater.*, **323**, 237 (2011).
24. K. C. Barick, M. Aslam, Y.-P. Lin, D. Bahadur, P. V. Prasad and V. P. Dravid, *J. Mater. Chem.*, **19**, 7023 (2009).
25. G. Yang, L. Tang, X. Lei, G. Zeng, Y. Cai, X. Wei, Y. Zhou, S. Li, Y. Fang and Y. Zhang, *Appl. Surf. Sci.*, **292**, 710 (2014).
26. M. Ozmen, K. Can, G. Arslan, A. Tor, Y. Cengeloglu and M.

Ersoz, *Desalination*, **254**, 162 (2010).
27. X. P. Yao, Z. J. Fu, Y. G. Zhao, L. Wang, L. Y. Fang and H. Y. Shen, *Talanta*, **97**, 124 (2012).
28. R. A. Bini, R. F. C. Marques, F. J. Santos, J. A. Chaker and M. Jafelicci, *J. Magn. Magn. Mater.*, **534-539**, 324 (2012).
29. T. V. J. Charpentier, A. Neville, J. L. Lanigan, R. Barker, M. J. Smith and T. Richardson, *ACS Omega* 1, **77-83**, 1 (2016).
30. V. Ganesan, C. Louis and S. P. Damodaran, *J. Environ. Chem. Eng.*, **2176-2190**, 2 (2018).
31. H. Iida, K. Takayanagi, T. Nakanishi and T. Osaka, *J. Colloid Interface Sci.*, **274-280**, 1 (2007).
32. Y. Wei, B. Han, X. Hu, Y. Lin, X. Wang and X. Deng, *Procedia Eng.*, **632-637**, 27 (2012).
33. Y. Bagbi, A. Sarswat, D. Mohan, A. Pandey and P. R. Solanki, *Sci. Rep.*, **7672**, 7 (2017).